

Enhancing the Flight Endurance and Autonomy of Multirotor UAVs Using Solar Power

AGHA, Stephen <<http://orcid.org/0000-0002-8069-2611>>, ABIDALI, Aly, VEPA, Ranjan and SHAHEED, M Hasan

Available from Sheffield Hallam University Research Archive (SHURA) at:

<https://shura.shu.ac.uk/37112/>

This document is the Accepted Version [AM]

Citation:

AGHA, Stephen, ABIDALI, Aly, VEPA, Ranjan and SHAHEED, M Hasan (2026). Enhancing the Flight Endurance and Autonomy of Multirotor UAVs Using Solar Power. IEEE Aerospace and Electronic Systems Magazine, 1-10. [Article]

Copyright and re-use policy

See <http://shura.shu.ac.uk/information.html>

Enhancing the Flight Endurance and Autonomy of Multirotor UAVs Using Solar Power

Stephen A. Agha, Aly Abidali, Ranjan Vepa, *Member, IEEE* and M. Hasan Shaheed, *Member, IEEE*

Abstract—This paper is focused on improving the flight endurance of a multirotor unmanned aerial vehicle (UAV) by utilizing a solar-battery hybrid energy system. This arrangement imparts energy autonomy to the system and in this study, an increase in endurance is achieved in real-world conditions. To achieve this result, an integrated design framework is introduced with the aim of sequencing the subsystem design with consideration for the interplay between the subsystems such that predefined performance specifications can be attained. This systematic approach was implemented in this study to realize a prototype solar-powered quadrotor which was subsequently tested outdoors, successfully. The increase in the flight endurance of the multirotor solar-powered UAV demonstrated in this article, presents an opportunity for increased scope for commercial and industrial applications.

Index Terms—Autonomy, Drone, Multirotor, Solar-Powered UAV, UAV

I. INTRODUCTION

With the maturing of the enabling technologies for multirotor unmanned aerial vehicles (UAVs), their popularity and applications have grown remarkably. Non-military applications now include industrial inspection, package delivery, environmental surveys, wildlife monitoring, photogrammetry, academic research as well as recreation and their impact can be extended with multiple UAVs in coordinated operation [1]. Compared with fixed-wing UAVs, rotary wing systems have the advantage of vertical take-off and landing (VTOL), omnidirectional and low-speed flight, greater maneuverability, and the ability to hover in place. These capabilities make multirotor UAVs the platform of choice for some of the aforementioned applications. Given the need for rotary-wing aircraft to expend energy to generate lift, multirotor UAVs have comparatively higher power demand than fixed-wing UAVs. The resulting lower flight endurance constrains the real-world use of multirotor UAVs. Hybrid UAVs offer the VTOL capability of rotary-wing UAVs coupled with superior flight endurance and speed of fixed-wing systems. Such systems pose increased complexity in configuration and operation. Flight control of multirotor and fixed-wing modes as well as

transitions between them has been demonstrated by Bauersfeld et al [2].

Traditional battery-only quadrotor UAVs typically have up to thirty minutes of flight time, flight durations between an hour and a half to four hours have been reported for hydrogen fuel cell-powered quadrotors [3], [4], [5], [6] and four and a half-hour flight endurance has been demonstrated for a gasoline-electric hybrid quadrotor [7]. Besides energy system considerations, other approaches utilized to increase flight endurance include the use of ducted fans to increase propulsion efficiency [8], utilizing gravitational potential energy via dynamic or thermal soaring [9]. Solar power poses a paradigm shift from carrying a finite energy supply at take-off to harvesting energy in-flight. This presents the possibility for flight endurance limited only by the availability of solar energy.

There is a rich history of implementing solar energy on fixed-wing UAV platforms including the pioneering Sunrise 1 by Robert Boucher in 1984 [10], the AtlantikSolar capable of multi-day flight, developed at ETH Zurich [11], [12] and the manned solar impulse which was flown around the world in 2016 [13]. Powering rotary-wing UAVs by the sun is relatively new given the large energy requirement and the challenge of solar panel placement on the aerial vehicle. The world's first purely solar-powered rotary-wing aircraft developed at Queen Mary University of London [14] demonstrated the feasibility of such a platform. However, for real-world applications, solar-powered rotary-wing aerial vehicles will require energy storage to smoothen out the variation in solar irradiance, ambient temperature, and power demand [15].

It is estimated that about 96% of commercial UAVs are battery-powered [13]. Batteries with higher energy densities are required to improve the flight endurance of such systems. According to K. P. Jain and M. W. Mueller [16] the flight endurance of a multirotor UAV is optimized for a given battery mass fraction. That is, increasing the battery size beyond a given optimal battery mass fraction will reduce the flight endurance as more energy is expended in carrying the extra battery weight. In-flight battery swapping has been demonstrated as a method of increasing the flight time of a multirotor [16]. This approach is constrained by the need for a

Article submitted on 26/05/2023. The first author wishes to acknowledge the financial support of the Niger Delta Development Commission (NDDC).

Stephen A. Agha is affiliated with the School of Engineering and Built Environment, Sheffield Hallam University, Sheffield, UK (s.gha@shu.ac.uk);

Aly Abidali (a.abidali@hotmail.com); Ranjan Vepa (r.vepa@qmul.ac.uk); and M. Hasan Shaheed (Corresponding Author m.h.shaheed@qmul.ac.uk) are affiliated with the School of Engineering and Material Science, Queen Mary University of London, London, UK.

motion capture system to enable precision docking of the ‘flying battery’ but also the logistics of continually providing charged batteries for the swap. Ultra-fast charging solutions are being developed and applied to minimize charge time and hence the need for battery swaps [3], [17]. Other solutions explored in the literature include aerial/mobile platform recharging [16], wireless charging – including the use of lasers [18], tethering the aerial vehicle to an energy source via a cable [5]. Compared to these alternatives, solar power offers the advantage of energy autonomy, hence, no field support infrastructure is required to reenergize the system once deployed.

Powering a multirotor UAV with solar energy presents challenges, the chief of which is achieving a suitably lightweight but sufficiently rigid design capable of flight. Furthermore, the low weight combined with a large surface area renders the UAV susceptible to wind disturbance and potential flight instability. These twin factors are considered in the conceptual design of a multi-rotor solar-powered UAV presented in this paper. This article therefore contributes to the body of knowledge by presenting a systematic approach to the design and development of solar-powered rotary wing aerial vehicles with due consideration of competing factors to balance subsystem design and selection with full system requirement. The stability of a UAV such as this can be improved by control algorithms such as the nonsingular terminal sliding mode control proposed by Nguyen et al [19]. Controller design and implementation is however outside the scope of the present article. The paper is organized as follows: a systematic design framework is presented next with an outline of the design objective followed by a description of an iterative design cycle and the design undertaken for individual sub-systems. Hardware implementation of a prototype and its subsequent testing are also detailed, followed by an evaluation of the final integrated system. Concluding remarks are given in the final section.

II. METHODS: SYSTEMATIC DESIGN FRAMEWORK

A. Design Objectives

The primary guiding objectives for the design of the solar-powered UAV are:

1. Stable flight regardless of ambient condition: operation in real-world conditions inexorably involves variations in solar irradiance, cell temperature as well as orientation. It is imperative that the UAV can remain airborne and stable irrespective of these variations.
2. Flight endurance extended beyond battery-only flight time; despite the added weight and aerodynamic drag from the solar panel. In addition to achieving energy autonomy, it is intended that the flight time of the Solar-hybrid UAV is longer than that of the battery-only system. Hence, the nominal power generated by the solar panel should offset the energy required to carry the extra load (inertia and aerodynamic) imposed by the panel.
3. Maneuverability for practical operation: while the power-to-mass ratio of solar panels becomes more favorable as the panel is scaled up, it is important to achieve a balance between the

power-to-mass ratio and the overall system size. The system mass and mass moment of inertia increase with an increase in system size and renders the UAV less agile. The aerodynamic drag experienced by the system also increases proportionally with the surface area of the solar panel.

4. Build simplicity: The system presented in this article may benefit from the application of advanced materials or optimization techniques, and specialist (lightweight or miniature) components. However, development was guided by considerations of simplicity and practicality of fabrication and assembly within budget. Where possible, commercially available hardware components were used to reduce development cost and time.

Guided by the above objectives, the broad design specifications for this system were:

- The overall mass of the system to be below 1.35 kg
- Achieve up to a 2:1 thrust to weight ratio.
- The solar panel should be able to supply up to 80% of the total power required at hover
- The energy storage capacity is sufficient to sustain flight for up to ten minutes
- To retain structural symmetry and minimize rotational inertia via the solar panel configuration
- The overall cost of the system should be low (<£1500).

The target mass was determined based on the sub-kilogram mass achieved with the 36-cell purely solar-powered system described by Shaheed et al [14]. The system developed in this paper includes energy storage resulting in a heavier system, hence the target mass sets a realistic compromise between competing aspects of the system design.

B. Iterative Design Cycle

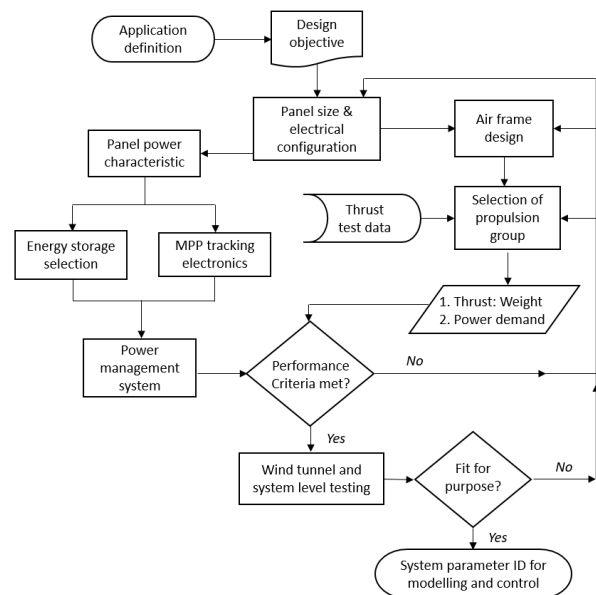


Figure 1: Iterative design cycle for development of solar-powered multi-rotor UAV

Given the interdependence of the Solarcopter subsystems, a framework for the systematic design of the solar-powered UAV was derived to guide the iterative design process. The design

framework presented in Figure 1 indicates the design hierarchy and dependencies between subsystem sizing and selection. Component sizing commences with the solar panel which is expected to contribute between 35% and 50% of the total system mass and is therefore a critical step to be considered ahead of designing the system support structure. As detailed in Figure 1, the panel size (and configuration) directly influences the battery voltage and hence, the appropriate motor-propeller combination to be used. The acceptance criteria for the design are directly related to the objectives and specifications presented in the preceding section.

C. Panel Design

The solar panel for this system is built up with SunPower™ C60 cells with sides of length 0.125 m and an effective surface area of 0.0152 m². Each cell has a maximum rated power of 3.42 W (22.5% efficiency) with voltage and current of 0.582 V and 5.93 A respectively [20] at maximum power. To permit testing different power extraction approaches it was essential for the cell voltage at maximum power to be close to the nominal battery voltage – 11.1 V (nominal voltage of a 3-cell lithium-ion polymer battery – 3-S). As the solar panel is composed of discrete solar cells of fixed size and shape, the geometric layout of the panel is constrained to have a composite

rectangular form. Square and cross-shaped configurations (see Figure 2) were considered for cell counts between 32 and 60.

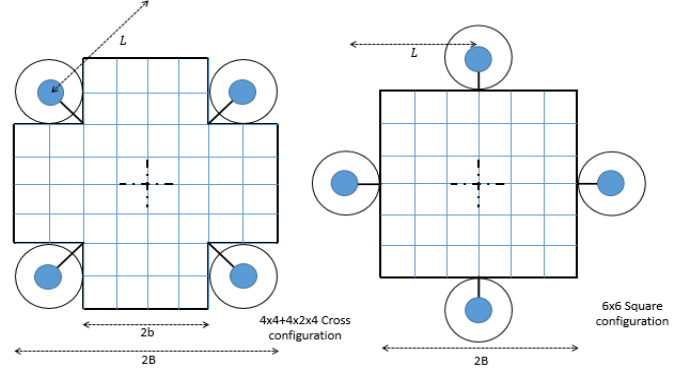


Figure 2: Geometric configurations for solar panel considered for symmetry and compactness.

Comparison of the different panel configurations was based on the size, inertia properties, and electrical power characteristics. N is the number of cells in a row (or column) of the square portion of the panel. M is the number of cells extending from the square portion of the ‘cross’ (+) configuration panel (see figure 2).

Table 1: Comparison of system characteristics estimated for a variety of solar panel configurations

| Cell rows in square portion (NxN) | Cells in Side panel layers (M) | Cell count | Panel max power [W] | Panel characteristic lengths [m] | | Minimum arm length, L [m] | System mass (without rotor or battery) [g] | UAV power to mass ratio [W/g] | Mass moment of inertia (I_{zz} through centroid) [kgm ²] | | |
|-----------------------------------|--------------------------------|------------|---------------------|----------------------------------|------|-----------------------------|--|-------------------------------|---|----------------|--------|
| | | | | B | b | | | | Panel | frame + motors | System |
| 4 | 1 | 32 | 109 | 0.41 | 0.28 | 0.60 | 478.9 | 0.229 | 0.028 | 0.095 | 0.124 |
| 3 | 2 | 33 | 113 | 0.48 | 0.21 | 0.51 | 470.0 | 0.240 | 0.032 | 0.066 | 0.098 |
| 6 | 0 | 36 | 123 | 0.41 | 0.41 | 0.56 | 496.0 | 0.248 | 0.037 | 0.083 | 0.119 |
| 5 | 1 | 45 | 154 | 0.48 | 0.34 | 0.70 | 613.8 | 0.251 | 0.056 | 0.131 | 0.187 |
| 4 | 2 | 48 | 164 | 0.55 | 0.28 | 0.60 | 622.9 | 0.264 | 0.065 | 0.095 | 0.161 |
| 7 | 0 | 49 | 168 | 0.48 | 0.48 | 0.63 | 625.6 | 0.268 | 0.068 | 0.106 | 0.174 |
| 6 | 1 | 60 | 205 | 0.55 | 0.41 | 0.80 | 766.7 | 0.268 | 0.099 | 0.174 | 0.274 |

The number of cells in a panel are computed as $N^2 + 4MN$ ($M = 0$ for square configuration). Panel characteristic lengths are $B = [(N + 2M) \times 0.125 \times 1.1]/2$ and $b = (N \times 0.125 \times 1.1)/2$. Where 0.125 is the length of the cell side and 1.1 accounts for spacing between panels. The power from the panel is estimated as the number of cells multiplied by 3.42 W. The minimum arm length is computed as $L = (b + 0.1524) \sqrt{2}/\kappa$, where 0.1524 is the anticipated propeller radius in meters and κ is 1 for the cross configuration and $\sqrt{2}$ for the cross configuration. The system mass is estimated as $M_{sys} = N_{cells} \times 7.5 \times 1.5 + \delta_f L \times 4 + 79.66$. The number of cells (N_{cells}) is as computed above, each cell has a mass of 7.5 g, 1.5 is used to account for the added mass of the panel support, the

linear mass density of the frame structure is $\delta_f = 46$ g/m and the avionics, connection etc. are accounted for as 79.66 g. For the square panel, the mass moment of inertia is computed as $I_{zz} = 8\gamma B^4/3$, and $I_{zz} = 8\gamma b[B^3 + Bb^2 - b^3]/3$ for cross configuration, where γ is the area density of the panel (see supplementary material for derivation). The moment of inertia contribution of the frame and rotor are computed as $I_{zz}^{f+r} = 4 \times [M_{rotor}L^2 + \delta_f L^3/3]$. M_{rotor} is the mass of a single motor.

As shown in Table 1, the comparison between configurations is based on the estimated panel power-to-system mass ratio (excluding the battery and rotors) and the mass moment of inertia. The general trend is for an increase in the power-to-mass ratio with an increase in panel size (cell count) which is expected given that the surface area of the panel increases while

its thickness remains constant. However, the rate of power density increase with cell count, reduces as the cell count increases. Single cell increase (from 32 to 33 cells), results in a 4.7% increase in power-to-mass ratio but only 1.5% when increased from 48 to 49 cells. No power-to-mass ratio increase is registered for an 11-cell increase from 49 to 60 cells. A small mass moment of inertia is desirable to achieve a more responsive and agile system.

The 1.5% increase in power density for the single cell increase to 49 cells is accompanied by a 4.5% increase in the moment of inertia of the panel and 7.8% when the frame and motors are included. In addition to these, a more suitable electrical configuration is achievable with 48 cells compared with the odd-numbered 7×7 cell configuration. A 48-cell panel configured as two 24-cell series panels that are connected in parallel will theoretically produce 13.97 V terminal voltage and

11.86 A at maximum power at 1000 W/m² irradiance under standard test conditions (STC). The operating voltage and current will inexorably vary with the prevailing ambient conditions; however, this voltage value is close to the open circuit voltage of a fully charged 3-cell lithium-ion battery (12.6 V). This panel configuration was therefore selected for the current system with a panel efficiency of 20.25%.

D. Mechanical Support Structure

The main structural components of the Solarcopter are the airframe and the panel support, both of which contribute significantly to the final system mass. The goal of the structural design is therefore to realize a suitably light-weight rigid structure capable of safely bearing both deadweight and the dynamic loads generated in-flight.

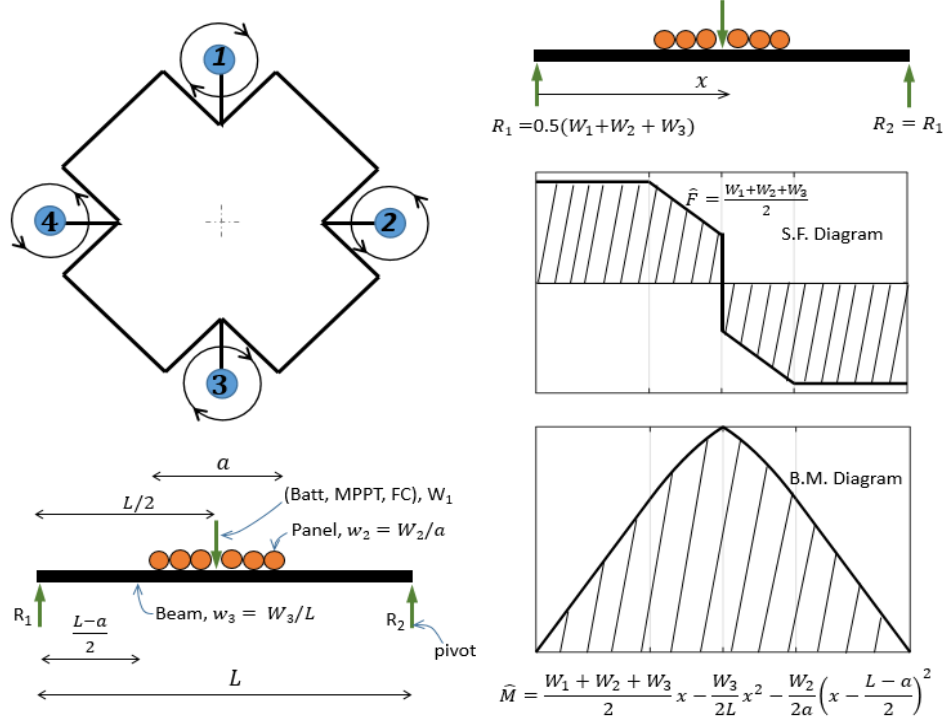


Figure 3: 2D approximation of Solarcopter loading with shear force and bending moment diagrams

Carbon fiber (CF) has been a material of choice for UAV frame design due to the combination of high material stiffness, high ultimate tensile strength, and low bulk density. A high structural stiffness and lightweight can be achieved, for the airframe, by using optimized space-truss structures, thin-walled tubes or H/I beam designed to maximize bending stiffness in a desired direction. While the space truss lends itself to extensive design optimization (compared to beams available in discrete sizes), assembling the space truss is quite time intensive. Selection of a beam cross-section for the frame design involves comparison of the geometric properties of the candidate cross-sections including the cross-sectional area, second moment of area and section modulus. Given that the same material is considered for all candidate cross-sections, the cross-sectional area is directly related to the linear density while the second moment of area is indicative of the flexural rigidity due to the geometric structure of the section. Furthermore, the section

modulus, Z , given by the ratio of the second moment of area, I , and the maximum distance from the neutral axis, y_{max} , ($Z = I/y_{max} = M/\sigma_{max}$) indicates the maximum bending moment, M , a section will experience when the maximum allowable bending stress, σ_{max} , is applied. The three candidate beam options considered were; a circular, square/rectangular and I-beam. Analysis indicates that for a similar cross-sectional area (hence weight), the square cross-sections generally have a smaller second moment of area compared with the circular profile. The square profile generally has a higher section modulus given its greater material concentration at extreme ends from the neutral axis. Therefore, for comparable masses (same material) the circular profile will possess greater bending stiffness, but the square profile will withstand greater bending moments before failure. (see Table S1 of supplementary material) Considering that the frame will experience

asymmetric loading, reduction in mass may be achieved by utilizing non-axisymmetric structural members such as rectangular and I-beam profiles. Although it is possible to engineer these non-axisymmetric cross sections for the required purpose, the search space was limited to commercially available profiles for simplicity. A 13 mm \times 6 mm rectangular CF beam available in 1 m lengths was chosen.

The suitability of the selected rectangular cross-section (and design material) is assessed via capacity to bear the design loads. This was achieved by idealizing the loading condition as a 2D simply supported beam with a combination of concentrated and uniformly distributed loads. Assuming symmetry, two arms of the Solarcopter will bear half the total weight of the aircraft with the rotors considered as simple supports. The load case comprises the mass of the batteries, flight controller and power electronics as a concentrated load, W_1 kg, acting through the midpoint of the beam. Half the solar panel mass, W_2 kg, is distributed over a distance, a m, and the mass of the beam, W_3 kg, is uniformly distributed along its length, L m. Figure 3 represents the idealized load case with corresponding shear force and bending moment diagrams. To evaluate the idealized beam, mass concentration at the center is estimated as 450 g ($W_1 = 225$ g). The solar panel mass is estimated at 500 g ($W_2 = 250$ g), acting uniformly over a distance of $a = 2b/\sin 45 = 0.78$ m, where $2b$ is the width of 4 cells with spacing in-between. The rectangular beam has a linear density, $w_3 = W_3/L$ of 0.0554 g/mm and the beam length,

L , is 1.21 m (then $W_3 = 67.03$ kg). Using these values, the maximum bending moment is $\hat{M} = 129.45$ g-m at the middle of the section and the maximum shear force is $\hat{F} = 271.02$ g at the supports. Given a section modulus, $Z_{xx} = 104.1$ mm³, and the cross-sectional area, $CA = 34.6$ mm², for the rectangular carbon fiber rod (see Table S1), the maximum bending stress, $\hat{\sigma}_B = \hat{M}/Z_{xx}$, and maximum shear stress, $\hat{\sigma}_S = \hat{F}/CA$, are evaluated as 12.15 MPa and 76.76 kPa respectively. This is about 30 times less than the lower limit for ultimate strength of the carbon fiber reinforced polymer (Table S2 of Supplementary Material [21], [22], [23]) and about 2.7 times less than that of Polylactide (PLA).

The Solarcopter frame comprises four rectangular carbon fiber rods joined at the center by a 3D-printed hub (made from PLA filament). These indicate that a central hub with similar wall thickness as the rods will be adequate to bear the Solarcopter loads with over 100% safety factor. However, the level of infill used when printing must be factored in, and adequate tolerance given.

The cells of the solar panel also require support to hold them in place and protect them from damage that can result from shock loading. Therefore, the supports are required to absorb some vibrational energy, and to also provide sufficient rigidity and strength to resist dynamic forces imposed by vehicle acceleration as well as air resistance. Thin paper laminated foam boards were chosen for this function. The panel support was designed with CAD software, laser cut and then assembled.

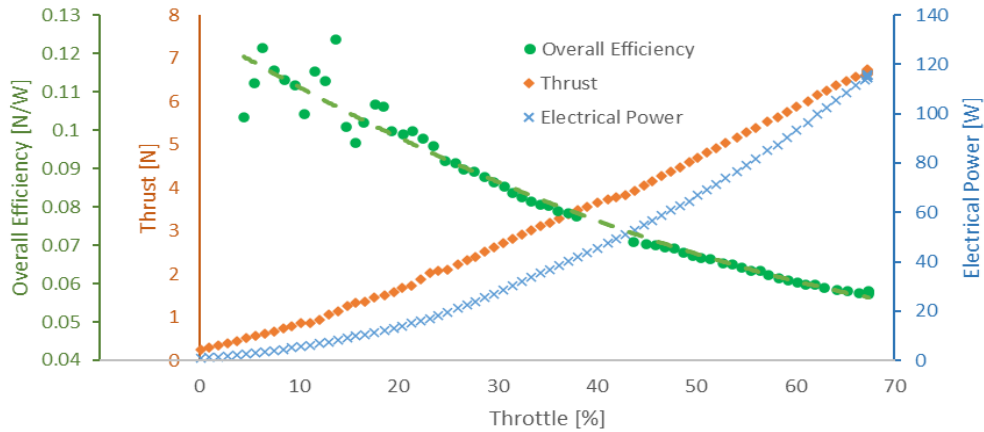


Figure 4: Variation of efficiency, thrust and power from a ramp test

E. Propulsion

In the selection of the motor-propeller pair for the present UAV, both efficiency and performance were considered simultaneously. Disc loading, given by the ratio of the total mass of an aerial vehicle to the swept area of its rotors, indicates an inverse quadratic relationship with the hover efficiency of the vehicle [24]. In general, better hover efficiency is achieved using a larger propeller spinning slowly compared to a smaller propeller with a higher angular velocity. However, except a gearbox is used; larger propellers require larger motors (for the higher torque requirement) both of which correspond to larger inertia contributions hence rendering the system less agile. Furthermore, the actuators should be able to react fast enough to provide corrections. To address these dual design needs, two

sets of experiments, a ramp test and a step response test, were performed on an array of propellers. The ramp test involved increasing motor input linearly from 0 to 70% of full throttle in 30 s, this throttle position is held constant for 5 s before ramping down at a constant rate to zero. Measurements taken during the ramp test include voltage, current, angular speed of motor, ESC signal, thrust and torque generated. The closed-loop response of the rotors shows first-order dynamics; hence a step response test is used to evaluate their time constant which provides an objective comparison of performance. Propellers with diameters between 11" and 14", corresponding to disc loadings of 5.30 and 3.27 kg/m², coupled with two different motors were tested and compared. Typical result plots for the ramp tests are shown in Figure 4.

Both the static and dynamic properties of the rotors were considered in making a final selection. Rotor selection was therefore based on the prediction of minimum electrical power input at hover. Also using a dynamic model of the UAV which included actuator dynamics, it was determined that the time constant of the selected rotor was within the limit for stability. A Turnigy® 2826 -1130 kV brushless outrunner motor with 14 poles, coupled with a 12"x 6" carbon fiber propeller was chosen for this application. This had a rotor mass of 61.5 g, power draw at hover of 42.1 W, a 90% settling time of 32 s and produced an estimated thrust to weight ratio of 2.76. Given the iterative nature of the design cycle, the rotor selection was checked after each subsystem design step which altered the system mass. A ducted fan design can improve rotor efficiency by reducing tip losses from the propeller blades when the clearance from the blades must be very small. However, this design was not used in this iteration to avoid the added mass of the ducts, especially given the significant distance from the center of rotation.

F. Energy Storage System

An energy storage device is required to balance out the mismatch in energy demand and supply thus enabling continuous flight regardless of prevailing ambient conditions. Selection criteria for the storage device are the rated voltage, maximum current rating, weight contribution and overall capacity. Lithium-ion-polymer batteries are the preferred energy storage device given their energy and power densities as well as their cycle efficiency and capacity for many charge-discharge cycles.

The selected motors are designed to operate with nominal voltages between 7.4 V and 11.1 V (2-cell and 3-cell LiPo batteries respectively). Thrust testing indicated superior motor performance with 3-cell battery voltage, hence this cell configuration was selected.

The battery capacity is determined based on the desired battery-only flight time and the mass contribution. The battery capacity is evaluated as the product of the current draw in amperes and the desired flight time in hours. The design point in this case is the current draw at hover (38% throttle with 3.7 A per rotor in this case). A 2200mAh battery estimated to provide 8.9 minutes of battery-only flight was selected.

The maximum continuous current discharge required of the battery was estimated from the current draw at 70% throttle (11.41 A per rotor). That is, a C-rating of 20.7 for a 2200mAh battery is required. The battery should also be able to deliver the burst current (sustainable for only 15 – 20 sec) corresponding to 100% throttle (extrapolated as 22.37 A per rotor). A burst current rating of 40.7 C is therefore required. The selected battery is rated 45 C. Finally, the allowable charge rate for the battery (10 C) was sufficient to accommodate the anticipated maximum current flow from the panel (14.8 A).

G. Power Electronics

For a UAV of this size, two distinct voltage levels are required for operation; a high voltage at the selected battery level used for propulsion and a stepped-down voltage, typically 5 V, for the avionics. The lower voltage was provided for this UAV using an off-the-shelf battery eliminating circuit (BEC) which is essentially a step-down switching voltage regulator. The type of electrical connection between the PV panel and the battery/load must be carefully considered for the protection it affords the battery, efficiency of power extraction from the panel and the mass contribution. Three methods were considered: direct coupling of the battery and load to the panel, utilization of a pulse width modulation charge controller and maximum power point tracking (see Figure 5 for Schematic). Each method was examined using a solar array simulator (SAS, Chroma® 62020H-150S programmable DC power supply) and a programmable electronic load (Applent® AT8612 DC). Two sets of tests were performed for each extraction method. The first is termed a static test as only a single set of I-V and P-V curves were used, and the load was kept constant. Static tests were run for 10 minutes at three solar irradiance levels (600, 800 and 1000 W/m²) with temperature set to 25 °C in all cases. The second experiment is a dynamic test in which the I-V and P-V curves of the SAS change in accordance with real-world solar irradiance and temperature data. The average irradiance and temperature values for this data set are 661.5 W/m² and 21.2 °C with maximum values of 751 W/m², 23.0 °C and minimum of 501 W/m², 17.3 °C, respectively (see Figure.S2 in Supplementary Figures [25]).

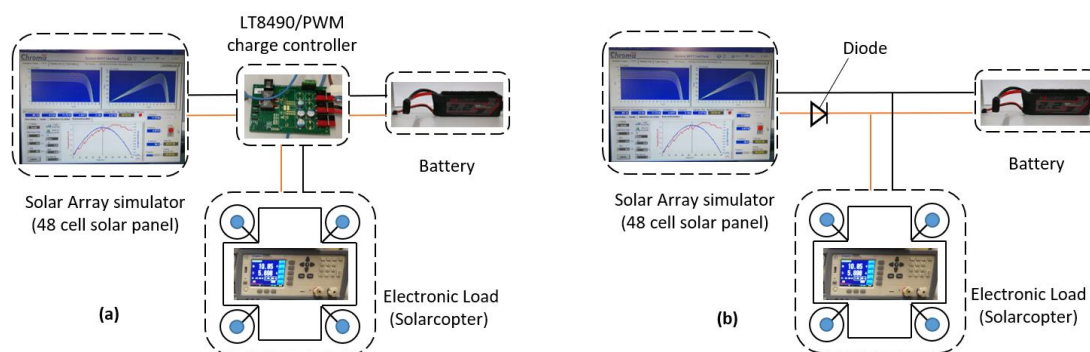


Figure 5: Block diagram of powering schemes. a. using a charge controller b. Direct coupling

The LT8490 demonstration board by Linear technology® was used for maximum power point tracking. It is a boost-buck

switching voltage regulator suitable for the LiPo battery chemistry as it utilizes a constant-current constant-voltage

charging profile [26]. It also has a proprietary perturb and observe (P&O) MPP tracking algorithm with intermittent full range voltage scan for global maximum power point tracking (GMPPT). As expected, the PWM and direct coupling approaches show similar results for the static test with higher efficiency at lower irradiance. Efficiencies for direct coupling were (93.73%, 90.26% and 88.31%) and for PWM were (93.53%, 90.58% and 88.11%) for (600 W/m², 800 W/m² and 1000 W/m²) irradiance levels, respectively. The operating voltages are also similar for these two methods as they are determined by the instantaneous battery voltage. The MPPT approach shows near constant efficiency (98.88% ± 0.12%) regardless of the I-V/P-V curve which are between 5 and 10 percentage points higher than the other two methods.

The results for the dynamic tests indicate efficiencies of 84.66% and 83.74% for the direct coupling and PWM methods respectively. Going by the static test results, extraction efficiencies greater than 90% would be expected given that the average solar irradiance for the test is less than 800 W/m². The MPPT charge controller, however, indicates similar extraction efficiency for both static and dynamic conditions with an average value of 98.33%. Given that the solar panel was configured such that V_{mpp} is close to the open-circuit voltage of the battery at full charge, the direct coupling approach presents a superior option to the PWM charge controller. This is further reinforced by the “no added mass” advantage of the direct coupling method. While the MPPT charge controller extracts more power than the direct coupling setup, it would add 93.5 g of extra mass to the final system if used. Hence to justify using the MPPT, the extra power harnessed by tracking the maximum power point should offset the power required to lift the added mass of the charge controller. The thrust test results for the chosen rotor indicated a hover efficiency of 0.117 W/g, therefore an extra 10.9 W of power is required to lift the LT8490 charge controller board at hover.

The dynamic test result indicates an extra 17.08 W of power can be extracted from the panel by the MPPT method compared with the direct coupling approach. In addition to this, the LT8490 remains operational even at voltages below that of the battery. The LT8490 MPPT charge controller is therefore the preferred option for power extraction. The direct coupling approach will however be a more practical option for a smaller system.

III. HARDWARE IMPLEMENTATION AND REAL-WORLD TESTING

A. Assembled Physical System

The assembled system had a total mass of 1,549 g: about 14.7% higher than the initial design estimate. The heaviest components were the solar panel and airframe which constituted roughly 35% and 22% respectively of the total. The breakdown of the components by mass is presented in Figure 6 and indicates that the final contribution of the fasteners, connectors and wiring were nontrivial.

Figure 7(a) shows the assembly of the electrical components which were placed as close to the center of rotation as practical to minimize their moment of inertia contribution. Also, the

battery and MPPT charge controller are attached to opposite sides of the frame to counterbalance their respective moments. The out-of-balance moment created by the battery which is heavier than the charge controller will be corrected by the flight controller. This is an undesirable situation as it invariably results in some motors running at a slightly higher speed than others.

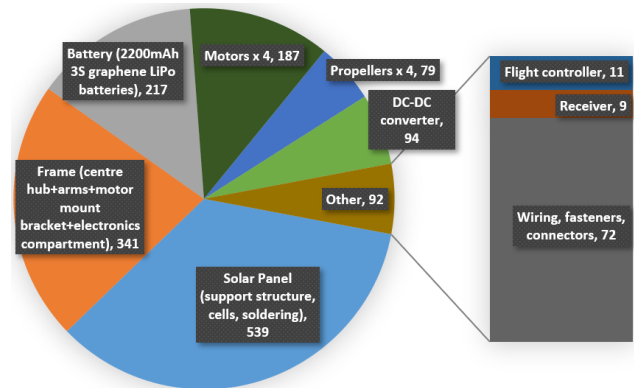


Figure 6: Actual mass contribution of Solarcopter components and subsystems. (Mass values displayed in grams)

Figure 7(b) is a top view of the fully assembled Solarcopter which was tested in phases. The system was first tested indoors while tethered to a solar array simulator. The rationale for this test was twofold; firstly, to function test the entire system to ensure the desired functionality of every subsystem. The second reason was to obtain real-time measurements of energy utilization from the solar array. With this test the ability of the flight controller to stabilize the UAV was observed.

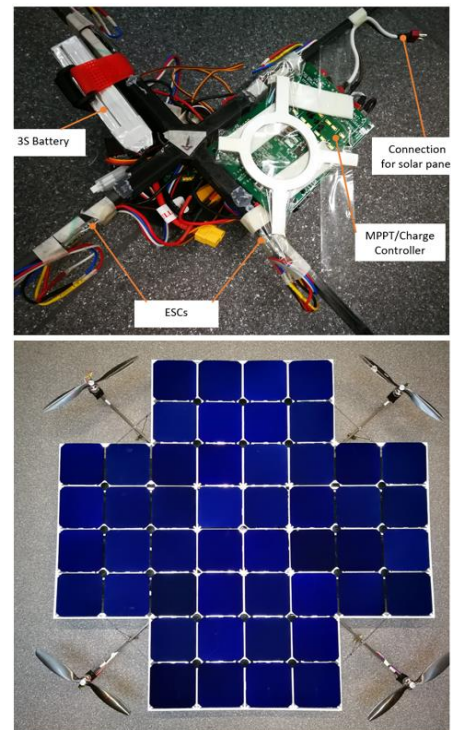


Figure 7: (a) Assembly of electrical components around central hub. (b) Top view of fully assembled Solarcopter

A series of real-world flight tests were conducted in July 2019. The test involved flying the UAV out of ground effect

and stabilizing it in hover flight under remote control. Figure 8 shows the Solarcopter in some of the test conditions encountered during outdoor flight tests. The Solarcopter recovered well from wind disturbances of as much as 6 m/s.

To stabilize the system during disturbance events, the rotors draw high currents which may exceed the maximum current deliverable by the solar panel. This extra electrical current requirement is met by the onboard battery. Hence, a purely solar-powered quadrotor UAV may be capable of sustained flight under controlled conditions but may have great difficulty operating in the presence of intermittent external disturbances.

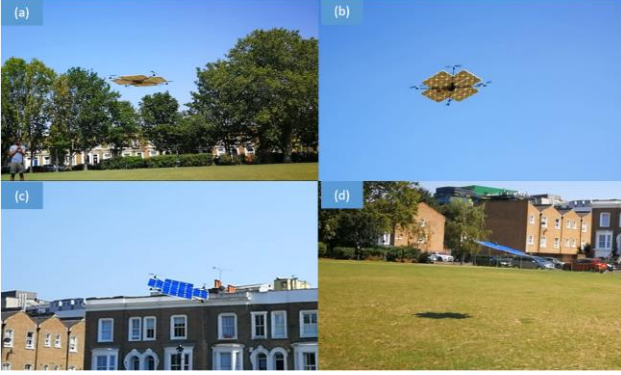


Figure 8: Outdoor flight test of the Solarcopter. (a) Hover flight, (b) Flight at high altitude (>10 m), (c) Flight in wind gust, (d) $\sim 16^\circ$ roll angle for translational motion.

B. System Evaluation

The eventual mass of the system was 14.7 % higher than predicted at the design phase. This translates to a higher power demand, however, based on the thrust experiment the maximum thrust to weight ratio is 2.49:1.

Given the increase in power requirement, the maximum solar panel output is only able to provide about 74.5% of the power required at hover.

Using the actual mass of the system, estimations of solar panel output power and thrust test data, the variation in flight endurance with the available solar irradiance can be estimated using the power balance equation.

$$T_{Flight} [min] = (B[Whr] \times 60 \frac{min}{hr}) / (C - S [W]) \quad (1)$$

Where, T_{Flight} is flight time in minutes B is the battery capacity, C is the energy consumed by the system and S is the power provided by the solar panel. Figure 9 shows the correlation between flight endurance and solar irradiance level for different battery capacities. The results indicate a maximum flight time of 28.9 minutes when the photovoltaic array is exposed to an average irradiance of 1 sun and maximum power is extracted. With the panel removed (less mass), the UAV is expected to fly for 13.0 minutes on battery power alone. The solar array generates sufficient power to offset the extra energy needed to lift its weight at 57.9% of maximum possible panel power. That is, the Solarcopter achieves a flight time similar to battery-only flight when it harnesses 579 W/m^2 of solar power. About 7.4 minutes of sustained flight is expected when there is no power contribution from the PV array (but the solar array and associated weight still present).

Given that it is unlikely to have continuous 1000 W/m^2 of irradiance, a more practical estimation of endurance can be obtained using real-world irradiance data such as was given in the power electronics section. For an average irradiance of 661 W/m^2 , the Solarcopter can remain airborne for 14.5 minutes. In practical operation, the power draw will vary with the UAV trajectory as well as the presence of disturbances. This is especially important for the Solarcopter as the drag experienced is proportional to the velocity and orientation of the system. Furthermore, the direction of the panel relative to the sun will also affect the amount of power generated by the solar array. These results are therefore indicative of the best-case scenario and outcomes will vary with prevailing ambient and operating conditions.

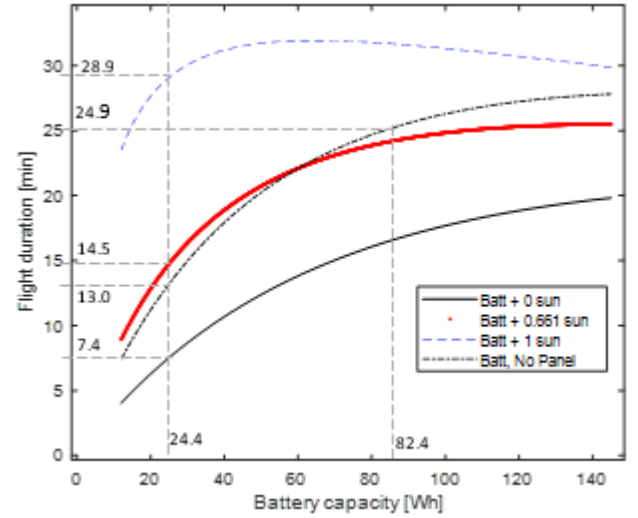


Figure 9: Variation of flight endurance with solar irradiance and battery capacity

If the entire mass of the panel was taken up by a battery (112.53 Wh/kg), the system is estimated to be capable of up to 24.9 minutes of flight on the resulting battery (82.4 Wh). While this is greater than the flight time achieved by the system at 661 W/m^2 , it is less than the maximum achievable flight endurance at 1 sun. The manufacturer of the 2200 mAh graphene LiPo battery used in the system specifies the maximum charge rate as 10C. Measurements from a solar array simulator for 600 W/m^2 and 1000 W/m^2 indicate charging rates of 3.4C (17.6 minutes) and 5.3C (11.3 minutes) respectively. It should be noted that the positive gradient of the initial portion of Figure 9 indicates the panel is unable to provide all the power required for flight even at 1 sun. In comparison to the purely solar-powered quadrotor presented by Hasan et al. [14] this current system poses a higher thrust to weight ratio and is capable of continuous operation regardless of prevailing irradiance conditions. While the system presented by Goh et al. [25] with 148-cell solar panel indicates the ability to operate in 882 W/m^2 , its surface area is about 3 times larger than the current system with an overall weight of 2607 kg. The comparatively high inertia property of the system severely limits the agility of the system, and the significant surface area renders it fragile and therefore impractical for real-world operation in the presence of wind disturbances. On the other hand, the micro-Solarcopter

developed by Abidali et al. [26] presents good agility, however, unfavourable scaling of solar panels for miniaturization, results in over three-fold increase in recharging time given its much smaller (13.8 times) battery capacity to panel surface area ratio.

C. Limitations, Future Work and Conclusion

Limitations of the present system include: the stiffness to weight ratio of the frame has not been optimized hence, weight savings can be made by utilizing an optimized space frame. The current frame was chosen for simplicity. The current system is not capable of operating in all weather. The electronics do not have protection from water, the paper laminated foam is not water-resistant. PLA has a relatively low glass transition temperature (about 60 °C) and short term ultraviolet light degradation resulting in discoloration and embrittlement from long term exposure to UV light. Hence alternative rapid prototyping materials such as PLA+, ASA, PETG or ABS are more suitable for more long-term testing.

Further work on this system includes analysis of the tolerance limits to wind disturbance which is an inexorable reality in outdoor operation and development of control algorithms for improved stability and disturbance rejection is vital. The concept of morphing the quadrotor arms [27] may provide an option for attitude stabilisation. Encapsulation of the solar panel will provide additional protection from the elements. In addition, UV resistant materials will be used in future iterations. Also, the aerodynamic characterisation of this UAV, including understanding the influence of the spinning rotor on the airflow around the solar panel, is an important step in system optimisation.

This article provides practical arguments for incorporating energy storage in rotary wing UAV operating in real-world conditions. A systematic approach to the design of solar-powered UAVs has been provided including the subsystem dependencies which must be considered. A flow chart outlining the interconnection of various subsystems, indicating a hierarchy of design and the iterative nature of the design process has been developed. Metrics for solar panel design and parameters for panel configuration selection have been presented. Characterization of the propulsion system to enable more objective decisions on conflicting performance metrics have been explored in this article. Also, the balance between energy storage capacity and onboard energy generation via solar cells have been considered for its impact on overall flight endurance. The systematic approach presented here has been applied to realize a working physical prototype to demonstrate the efficacy of the approach. The system reported in this article has a 2.49:1 thrust to weight ratio with a solar panel capable of providing up to 74.5% of the power required at hover. With an irradiance of 578 W/m² or more, flight endurance is enhanced beyond battery only operation. An irradiance of 600 W/m² allows the battery to be recharged in under 20 minutes thus imparting energy autonomy to the system.

REFERENCES

- [1] S. Mart'inez, M. Mart'inez, J. Cortés, and F. Bullo, "Motion Coordination with Distributed Information OBTAINING GLOBAL BEHAVIOR FROM LOCAL INTERACTION," 2007.
- [2] L. Bauersfeld, L. Spannagl, G. Ducard, and C. Onder, "MPC Flight Control for a Tilt-Rotor VTOL Aircraft," *IEEE Trans Aerosp Electron Syst*, vol. 57, no. 4, pp. 2395–2409, Aug. 2021, doi: 10.1109/TAES.2021.3061819.
- [3] A. M. Mazur and R. Domanski, "Hybrid energy systems in unmanned aerial vehicles," *Aircraft Engineering and Aerospace Technology*, 2018, doi: 10.1108/AEAT-08-2018-0218.
- [4] Z. F. Pan, L. An, and C. Y. Wen, "Recent advances in fuel cells based propulsion systems for unmanned aerial vehicles," *Appl Energy*, vol. 240, no. February, pp. 473–485, 2019, doi: 10.1016/j.apenergy.2019.02.079.
- [5] J. Dutczak, "Compressed hydrogen storage in contemporary fuel cell propulsion systems of small drones," *IOP Conf Ser Mater Sci Eng*, vol. 421, no. 4, 2018, doi: 10.1088/1757-899X/421/4/042013.
- [6] K. O. Sylvester, "Fuel cells extend flight time on drones," *Danish Technological Institute*, 2017. <https://www.dti.dk/fuel-cells-extend-flight-time-on-drones/37268> (accessed Feb. 07, 2018).
- [7] N. SUAS, "Skyfront Sets World Record for Drones with 4 hour and 34 minute flight," 2017. <https://www.suasnews.com/2017/09/skyfront-sets-world-record-for-drones-with-4-hour-and-34-minute-flight/> (accessed Jan. 31, 2018).
- [8] T. Zhang and G. N. Barakos, "Review on ducted fans for compound rotorcraft," *Aeronautical Journal*, vol. 124, no. 1277. Cambridge University Press, pp. 941–974, Jul. 01, 2020. doi: 10.1017/aer.2019.164.
- [9] G. D. Bousquet, M. S. Triantafyllou, and J. J. E. Slotine, "Optimal dynamic soaring consists of successive shallow arcs," *J R Soc Interface*, vol. 14, no. 135, Oct. 2017, doi: 10.1098/rsif.2017.0496.
- [10] J. (Astro F. Inc.) Robert Boucher, "History of Solar Flight AIAA/SAE/ASME 20th Joint Propulsion Conference," in *AIAA/SAE/ASME 20th Joint Propulsion Conference*, Cincinnati, Ohio, 1984, pp. 1–22. [Online]. Available: <http://astrobbob.com/solarhistory.pdf>
- [11] P. Oettershagen et al., "Design of small hand-launched solar-powered UAVs: From concept study to a multi-day world endurance record flight," *J Field Robot*, vol. 34, no. 7, pp. 1352–1377, 2017, doi: 10.1002/rob.21717.
- [12] P. Oettershagen et al., "A Solar-Powered Hand-Launchable UAV for Low-Altitude Multi-Day Continuous Flight," *IEEE International Conference on Robotics and Automation (ICRA)*, pp. 3986–3993, 2015, doi: 10.1109/ICRA.2015.7139756.
- [13] BBC, "Solar Impulse lands in California after Pacific crossing," 2016. <http://www.bbc.co.uk/news/science-environment-36122618> (accessed Apr. 28, 2016).
- [14] M. H. Shaheed et al., "Flying by the Sun only: The Solarcopter prototype," *Aerosp Sci Technol*, vol. 45, pp. 209–214, 2015, doi: 10.1016/j.ast.2015.05.016.
- [15] N. Kingry et al., "Design, Modeling and Control of a Solar-Powered Quadcopter," *Proc IEEE Int Conf Robot Autom*, pp. 1251–1258, 2018, doi: 10.1109/ICRA.2018.8462896.
- [16] K. P. Jain and M. W. Mueller, "Flying batteries: In-flight battery switching to increase multirotor flight time," Sep. 2019, [Online]. Available: <http://arxiv.org/abs/1909.10091>
- [17] B. Kang and G. Ceder, "Battery materials for ultrafast charging and discharging," *Nature*, vol. 458, no. 7235, pp. 190–193, 2009, doi: 10.1038/nature07853.
- [18] Q. Zhang, W. Fang, Q. Liu, J. Wu, P. Xia, and L. Yang, "Distributed Laser Charging: A Wireless Power Transfer Approach," *IEEE Internet Things J*, vol. 5, no. 5, pp. 3853–3864, 2018, doi: 10.1109/JIOT.2018.2851070.
- [19] N. P. Nguyen, H. Oh, and J. Moon, "Continuous Nonsingular Terminal Sliding-Mode Control with Integral-Type Sliding Surface for Disturbed Systems: Application to Attitude Control for Quadrotor UAVs under External Disturbances," *IEEE Trans Aerosp Electron Syst*, vol. 58, no. 6, pp. 5635–5660, Dec. 2022, doi: 10.1109/TAES.2022.3177580.
- [20] SunPower Corp, "C60 Solar Cell Mono Crystalline Silicon," Sunpower Corporation. pp. 3–4, 2010.
- [21] P. D. Soden and R. D. Mcleish, "Variables affecting the strength of balsa wood," *J Strain Anal Eng Des*, vol. 11, no. 4, pp. 225–234, 1976, doi: 10.1243/03093247V114225.
- [22] Michael. F. Ashby, *Material and the Environment: eco-informed material choice*, First. Oxford, UK: Butterworth-Heinemann/Elsevier, 2009.
- [23] G. Newaz, M. Mayeed, and A. Rasul, "Characterization of balsa wood mechanical properties required for continuum damage mechanics

analysis,” Proceedings of the Institution of Mechanical Engineers, Part L: Journal of Materials: Design and Applications, vol. 230, no. 1, pp. 206–218, 2016, doi: 10.1177/1464420714564711.

- [24] Krossblade-Aerospace, “Disc loading and hover efficiency,” 2019. <https://www.krossblade.com/disc-loading-and-hover-efficiency> (accessed Aug. 09, 2019).
- [25] London Grid for Learning, “No Title,” 2019. <http://weather.lgfl.org.uk/qtables.aspx?sid=52&pid=1-19&day=30> (accessed Jun. 28, 2019).
- [26] Linear Technology Corporation, “LT8490 - High Voltage, High Current Buck-Boost Battery Charge Controller with Maximum Power Point Tracking (MPPT),” 2014. [Online]. Available: www.linear.com/LT8490



Stephen A. Agha Received the BEng in Mechanical Engineering from University of Port Harcourt, Rivers State, Nigeria in 2010, the MSc. Eng Advanced Mechanical Engineering from the University of Leeds, UK in 2013 and the PhD in Mechanical Engineering from Queen Mary University of London in 2020.

Between 2011 and 2012, he was a Field Engineer with Xenergi Oilfield Services where he pioneered the multi-zone perforation approach for well completion. He was an associate technical professional with Halliburton Energy Services between 2014 to 2015. He is currently a senior lecturer in the School of Engineering and Built Environment at Sheffield Hallam University, UK. His research interests are in the field of applied dynamics and control systems, with specific applications to unmanned aerial vehicles and driverless cars.

Dr. Agha is a chartered engineer and a member of the Institution of Mechanical Engineers (IMechE).



Aly Abidali received an MEng in aerospace engineering from the School of Engineering and Materials Science at Queen Mary University of London in 2013. He then obtained his PhD also in aerospace engineering in 2019. His research interests are in the field of aerial robotics and alternative energy. He is currently a senior

Mechanical Engineer at Utonomy Ltd.



Ranjan Vepa (M'06) Dr. Ranjan Vepa is a Reader in Aerospace Engineering in the School of Engineering and Material Science, Queen Mary, University of London.

His research interests include the design of control systems, and associated signal processing with applications in aerospace systems, smart structures, space-robotics, energy, and biomedical systems. In particular, the research interests include dynamics, robust estimation and control of linear and nonlinear aerospace, energy, and propulsion systems, flow control systems, trajectory optimization, and trajectory tracking. His current research focus is on the control of aerospace systems based on computational models and on the control and optimization of aerospace propulsion. He teaches master's level courses on Advanced Spacecraft Design, Aircraft Flight Control, and Simulation, Aeroelasticity, and Robotics. He is the author of seven books.

Dr Vepa is a Chartered Engineer (CEng). He is also a Member of the Royal Aeronautical Society, London, and a Fellow of the UK's Higher Education Academy.



M. Hasan Shaheed (M'03) Dr Shaheed received his PhD degree from the Automatic Control and Systems Engineering, University of Sheffield in 2001 in the field of flexible robotics. He is currently a Reader in Modelling and Control at the School of Engineering and Materials Science, Queen Mary University

of London, UK.

Over the years, he has published over 80 peer-reviewed articles and co-authored a book and several book chapters. He is an expert in the design, modelling, fabrication, control, and optimization of Robotic/Autonomous and Hybrid Renewable Energy Systems (RAS and HRES). The specific application areas of his research include aerial/solar aerial robots for monitoring and inspection, leader-follower robots for industrial processing and remote handling, robotic retractors with soft materials-based graspers for surgical applications, prosthetics, and hybrid renewable energy systems comprising photovoltaics, wind turbine, and pressure retarded osmosis. His research is supported by several industries and UK leading funding agencies.

Dr Shaheed is a Chartered Engineer (CEng), a member of the Institution of Engineering and Technology (IET), a Senior Fellow of the Higher Education Academy (SFHEA), UK and a recipient of the UK's prestigious National Teaching Fellowship (NTF).